Asian Journal of Research and Reviews in Physics

4(2): 6-20, 2021; Article no.AJR2P.66815
ISSN: 2582-5992

Instantaneous Ionospheric Scintillation Mapping over the East African Region by use of GPS Derived Amplitude Scintillation Proxy

Emirant Bertillas Amabayo[1,2*], Geoffrey Andima[1] and Richard Cliffe Ssenyunzi[1]

[1] *Department of Physics, Busitema University, Tororo, Uganda.*
[2] *Department of Physics, Mbarara University of Science and Technology, Mbarara, Uganda.*

Authors' contributions

This work was carried out in collaboration among all authors. GA and EBA designed the study, performed the analysis, wrote the protocol and wrote the first draft of the manuscript. RCS managed the literature searches. All authors read and approved the final manuscript.

Article Information

DOI: 10.9734/AJR2P/2021/v4i230138
Editor(s):
(1) Prof. Shi-Hai Dong, National Polytechnic Institute, Mexico.
Reviewers:
(1) Surendra Sunda GNSS, Airports Authority of India, India.
(2) Volkan AKGUL, Zonguldak Bulent Ecevit University, Turkey.
(3) Hai Wang, Beijing University of Posts and Telecommunications, China.
Complete Peer review History: http://www.sdiarticle4.com/review-history/66815

Received 02 February 2021
Accepted 08 April 2021
Published 21 April 2021

Original Research Article

ABSTRACT

Ionospheric scintillation activity over the East African region is often monitored using measurements from the SCIntillation Network Decision Aid (SCINDA) receivers. Many of the SCINDA receivers over East Africa are currently not archiving data and therefore a large part of the region remain un sampled. We investigated the possibility to use dual frequency receivers of the Global Navigation Satellite System (GNSS) network for scintillation mapping. A proxy for amplitude scintillation was first derived by scaling the rate of change of total electron content index (ROTI). The proxy was validated against S4 derived from nearly collocated SCINDA receivers over the region. A good correlation was observed between the proxy and S4. The proxy was then used to map the occurrence of amplitude scintillation over East Africa based on semivariogram modeling and Kriging interpolation technique. The results indicate that the S4 values had a good positive correlation with

**Corresponding author: E-mail: emirant.amabayo@gmail.com;*

the simulated S4p from the Kriging interpolation. This observation suggests that data from the dual frequency receivers of GNSS may be used to map scintillation over East Africa. These maps can in turn be used to study the evolution of ionospheric scintillation patterns over the region.

Keywords: Amplitude scintillation proxy; Scintillation maps; Kriging.

1 INTRODUCTION

The ionosphere plays a critical role in the propagation of trans-ionospheric radio signals. After the end of selective availability in 2000, the reliability and accuracy of systems that use trans-ionospheric radio signals such as the GNSS, apart from the hardware problems depend on the state of the ionosphere. The primary effect of the ionosphere on trans-ionospheric radio signal is the induced propagation time delay which depends on the signal frequency. Several methods e.g. [1, 2, 3] are available for correcting the effects that a user may experience due to ionospheric time delay of the GNSS signals. A typical, but still unresolved threat to GNSS users is the rapid and random variations in the amplitude and phase of satellite signals, commonly referred to as scintillation. It is generally known that ionospheric scintillation of a radio wave is caused by a plasma density irregularity lying along the signal path. The irregularity induces fluctuations in the phase and amplitude of the original signal by either refractive or diffractive scatter thus giving rise to a randomly modulated wavefront that is received on ground. Such rapid fluctuations disrupt communication along some satellite links. Phase fluctuations may result in cycle slips, thus affecting the receiver's ability to hold lock on a signal. Deep signal fades below the receiver's lock threshold often occur during strong amplitude fluctuations [4]. Both phase and amplitude fluctuations cause difficulties in the receiver's ability to remain locked on to the signal. The net effect is an increase in the noise level in the received signal, and inability of the receiver to smoothen the range measurements.

Ionospheric scintillation cannot be eliminated before the radio signal reaches the receiver's tracking loop. The remedy to scintillation is to avoid the times and the locations when it is most likely to occur. For this to be effective, accurate prediction of these times and places in real time is required. However, no such perfect systems are known to exist in the real world. Through continuous monitoring of scintillation characteristics, and analysis of available scintillation data in the archives, coded schemes have been developed to predict the likely times of communication outages due to scintillation. These codes are commonly referred to as models, and are derived from empirical e.g. [5], semi-empirical e.g. [6], and non-empirical techniques e.g. [7]. These models have produced results in good agreement with observations. No single model can perfectly predict scintillation at all times, frequencies and locations. The empirical and semi-empirical models are limited to the radio frequency, and geomagnetic regions for which they have been constructed [5]. The accuracy of theoretical models depends on the assumptions and approximations used to simplify the models [4, 8].

The SCINDA forecasting campaign of the Air Force Research Laboratory (AFRL), has a network of sensors deployed over Africa and South America to monitor ionospheric scintillation. Remotely stored data from these sensors are retrieved to produce amplitude scintillation index (S4), and phase scintillation index (σ_ϕ). Real-time scintillation maps are produced from these indices to advise users on the likelihood of communication outages. Though largely successful, the capability of SCINDA is limited by many factors [9]. Among these factors include the poor geographical distribution of the receivers and high maintenance costs which degrade the accuracy of the scintillation forecasts. The possibility of using scintillation proxies derived from the dual frequency GNSS receivers has been explored in the last two decades to overcome the limited geographical coverage offered by standard scintillation monitors [10, 11, 12, 13, 14]. In these studies a good correlation has been observed between the scintillation indices and the proxies suggesting that dual frequency receivers of GNSS network

could be used to characterize scintillation, especially in the absence of scintillation monitors. The current research in this area is focused towards refining these proxies to obtain a more appropriate scintillation proxy. Recently, [15] used irregularity drift velocity estimated from the nearby VHF receiver to derive a proxy for S4. Their results show that with a correct estimate of the irregularity drift velocity and the satellite velocity at the Ionospheric Pierce Point (IPP), a better match is observed between the S4 and the proxy values. The main objective of this paper is therefore to investigate the possibility to use the relatively low cost dual frequency GNSS receivers to map scintillation over East Africa. The wider geographical coverage provided by the relatively denser network of the GNSS receivers is expected to result in improved scintillation maps over the region.

2 DATA AND METHODS

2.1 Sources of Data

This study made use of data from both SCINDA and dual frequency GNSS receivers which form part of the ground receiver network over the East African region. The SCINDA network of receivers in East Africa were supplied by the Air Force Research Laboratory in coordination with Boston College, USA. While the GNSS receivers from which the data were obtained belong to either the International GNSS Service (IGS) network or the University NAVstar COnsortium (UNAVCO). Fig. 1 shows the location of the receivers from which data used in this study were obtained.

These data were processed to obtain the amplitude scintillation proxy which was then used to construct scintillation maps.

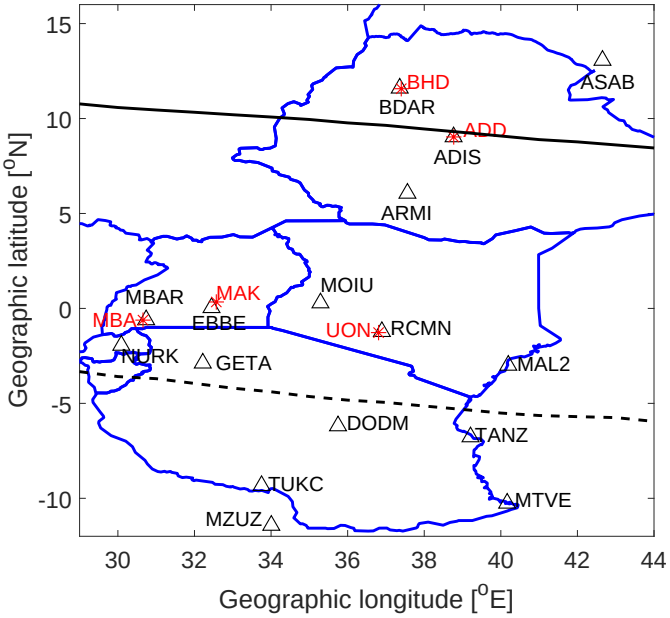

Fig. 1. Location of ground receiver infrastructure over East Africa from which data used in this study were obtained. The triangles are for the dual frequency GPS receivers while the asterisk are for the SCINDA receivers. The solid black and broken lines are the geomagnetic equator and the location of the southern crest of the Equatorial ionization anomaly respectively

2.2 Methods

2.2.1 Amplitude scintillation proxy index

The GNSS data in Receiver INdependent EXchange (RINEX) format were obtained from the selected stations over the East African region which are shown in Fig. 1. The total electron content (TEC) along the line-of-sight commonly referred to as slant TEC (sTEC) was extracted from the RINEX data using the GPS-TEC algorithm of Boston College [16]. The sTEC is defined as

$$\text{sTEC} = \int_R^S N_e ds, \tag{1}$$

where R and S are the receiver and satellite positions respectively and N_e is the electron density. The software uses the thin-shell mapping function to map the sTEC to obtain the TEC above the receiver often times referred to as vertical TEC (vTEC) as

$$\text{vTEC} = \text{sTEC} \times \left[1 - \left(\frac{R_E \text{sin}\ z_o}{R_E + h}\right)^2\right]^{\frac{1}{2}}, \tag{2}$$

where R_E and h are the radius of the earth and height of the ionosphere respectively, and z_o is the zenith angle at the observation site. The vTEC values were used to calculate the rate of change of TEC (ROT). The ROT for each satellite was detrended for elevation angles greater than 50^o to minimize the effects of large-scale gradients in TEC, which are not necessarily associated with irregularities [17]. The standard deviation of the detrended ROT was then calculated over a running window of 5 minutes to obtain ROT index (ROTI) [10]. The amplitude scintillation proxy (S4p) used in this study was then obtained by scaling ROTI following [12] as

$$\text{S4P} = \gamma \text{ROTI}. \tag{3}$$

The scaling factor γ in equation 3 is given by $\gamma^{-1} = 2\pi V^2/\lambda^2 r_e z$, where r_e is the electron radius (2.8×10^{-15} m), λ is the wavelength for the GPS L1 frequency and z is the scattering height which is taken to be 350 km. The unknown velocity V is given in [15] as

$$V = V_d - (V_{py} - \tan\theta \sin\phi V_{pz}), \tag{4}$$

where V_d is the zonal drift velocity of irregularities, V_{py} and V_{pz} are the ray path velocities in magnetic eastward and downward directions respectively and are determined from the satellite receiver geometry. The angles θ and ϕ are the nadir and the azimuth angles at the IPP respectively. We then used the derived proxy from equation 3 to construct amplitude scintillation maps over East Africa using the Kriging interpolation technique.

2.2.2 Kriging

Kriging is a well known method in geostatistics and dates to the pioneering work of Krige [18] in which he estimated the concentration of gold and other metals in the ore. Since then Kriging technique is widely used in environmental studies especially where there is a desire to interpolate a sparse data such as in mining, geology, remote sensing, and public health [19]. In ionospheric physics, Kriging has been applied in TEC mapping e.g. [20, 21] and mapping of ionospheric scintillation e.g. [22, 23, 24]. Unlike other methods of ionospheric mapping such as tomography that require a dense receiver network, Kriging operates on the sparse measurements and searches for the optimal covariance between the measurements. The estimate is based on two main assumptions of intrinsic stationarity in the expectation values of the measurements, and the variance of the measurements only depend on the distance between the measurements [20, 21]. The mathematical equivalence of these assumptions are

$$\begin{aligned} &E(z(x_i + h) - z(x_i)) = 0 \\ &\text{Var}(z(x_i + h) - z(x_i)) = 2\gamma(h), \end{aligned} \tag{5}$$

where h is the straight line distance between the measurements, $z(x_i)$ is the value of the variable which for our case is the S4p at position x_i and $z(x_i + h)$ is the S4p at position $x_i + h$. The function $\gamma(h)$ is called the semivariogram and it characterizes the spatial correlation of the S4p. The purpose of the Kriging technique is to estimate an unknown value z_o at x_o using a linear combination of the known values z_i at positions x_i as

$$z_o = \sum_i \lambda_i z_i, \tag{6}$$

where λ_i are the Kriging weights that are applied to each value of z_i at x_i. For the estimate in equation 6 to be unbiased, $\sum_i \lambda_i = 1$. The variance of the difference between the predicted value in equation 6 and the true value is

$$Var\left[\sum_i \lambda_i z(x_i) - z(x_o)\right] = 2\sum_i \lambda_i \gamma(x_i - x_o) - \sum_i \sum_j \lambda_i \lambda_j \gamma(x_i - x_j) - \gamma(x_o - x_o), \tag{7}$$

where $\gamma(x_i - x_o)$ is the semivariance of z between the sampling point x_i and the target point x_o and $\gamma(x_i - x_j)$ is the semivariance between the i^{th} and j^{th} sampling points. The Kriging equation is set by minimizing the variance in equation 7 subject to the constraint $\sum_i \lambda_i = 1$. From equations 6 and 7, and following [19], the Kriging equation is

$$\sum_i \lambda_i \gamma(x_i - x_j) + \psi = \gamma(x_i - x_o), \qquad \text{for all } j \tag{8}$$

where ψ is the Lagrange multiplier for minimization. The matrix form of equation 8 is

$$\begin{bmatrix} \gamma_{11} & \gamma_{12} & \cdots & \gamma_{1N} & 1 \\ \gamma_{21} & \gamma_{22} & \cdots & \gamma_{2N} & 1 \\ \vdots & \vdots & \ddots & \vdots & \vdots \\ \gamma_{N1} & \gamma_{N2} & \cdots & \gamma_{NN} & 1 \\ 1 & 1 & \vdots & 1 & 0 \end{bmatrix} \begin{bmatrix} \lambda_1 \\ \lambda_2 \\ \vdots \\ \lambda_N \\ \psi \end{bmatrix} = \begin{bmatrix} \gamma_{1o} \\ \gamma_{2o} \\ \vdots \\ \gamma_{No} \\ 1 \end{bmatrix} \tag{9}$$

In order to construct the interpolation in equation 6, the Kriging algorithm solves equation 9 for the values of λ_i and ψ. To solve equation 9, a semivariogram is required. For $N(h)$ pair of measurements at a distance h, and using equation 5, the semivariogram $\gamma(h)$ is given as

$$\gamma(h) = \frac{1}{2N(h)} \sum_{i=1}^{N(h)} \left[z(x_i + h) - z(x_i)\right]^2. \tag{10}$$

First, an experimental semivariogram was determined by substituting the values of S4p in equation 10 to examine the spatial variability of amplitude scintillation. The most appropriate theoretical semivariogram that best matched the experimental semivariogram is then determined. The theoretical semivariogram is then used in solving the Kriging equation and consequently an interpolated value of S4p is obtained in the un sampled points using equation 6.

3 RESULTS

3.1 Derivation and Validation of S4p

The intensity of scintillation experienced by a trans-ionospheric radio signal intercepted by moving irregularities has been reported to depend on the IPP velocity and the zonal drift velocity of the irregularities [25]. Following [15], we used the IPP velocity together with the zonal drift velocity of irregularities to scale ROTI according to equation 3 to obtain S4p. The zonal drift velocity of irregularities were obtained from VHF antennas in an east-west alignment nearly collocated with the dual frequency GNSS receivers. Fig. 2 shows the results for some satellites designated by their Pseudo Random Noise (PRN) numbers on the Day Of the Year (DOY) 219 and 300 in 2011 observed over Nairobi.

Fig. 2 (a) shows a case of weak scintillation over Nairobi with the S4 index recorded by PRN 14 reaching a value of 0.3 on the DOY 219 in 2011 between ∼21:30 LT and 22:30 LT. At the same time, the east-west velocity of the irregularities estimated from the VHF receiver at Nairobi was about 100 m/s. Relatively strong TEC fluctuations with the ROTI index reaching 1.5 TECU/min were also observed on the link of PRN 14 at high

elevation angles between 21:30 LT and 22:30 LT, suggesting that these fluctuations are not as a result of multipath. The trends of ROTI and S4 were similar. The values of S4p are in the same range as that of S4 though in some cases S4p under estimated S4 especially at lower elevation angles. Fig. 2(b) shows a case when scintillation was observed over Nairobi by PRN 11 at high elevation angles on the DOY 300 in 2011 from 20:40 LT to 23:00 LT. The estimated irregularity drift velocity at this time from the collocated VHF receiver was about 120 m/s to 135 m/s. The TEC showed strong fluctuations with the ROTI index reaching 3 TECU/min between 20:40 LT and 23:00 LT. During this time, strong scintillation of the signals from PRN 11 were observed with the S4 reaching 0.6. Although small variations were observed between S4p and S4, they are numerically close and they can easily be presented on the same axes. These observations suggest that S4p may be used to characterize scintillation similar to S4. However the use of S4p for characterizing scintillation over the East African region is hampered by the limited data for the zonal drift velocity of the irregularities over the region. In an attempt to address this challenge, we first analyzed the nighttime zonal drift velocity of irregularities over East Africa recorded by two VHF receivers one at Makerere and the other at Nairobi to obtain the most appropriate zonal drift velocity of irregularities over the region. Fig. 3 shows the variation of the hourly averaged zonal drift velocity of irregularities and the hourly occurrence probability of amplitude scintillation from collocated SCINDA receivers.

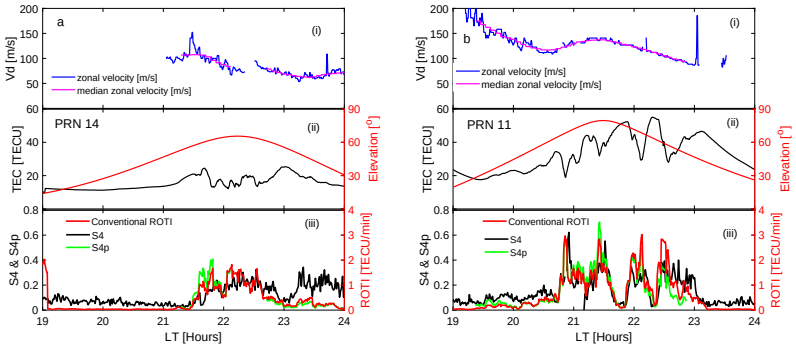

Fig. 2. Variation of zonal irregularity drift velocity (a(i) & b(i)), TEC (a(ii) & b(ii)), ROTI and S4 (a(iii) & b(iii)) over Nairobi for PRN 14 on DOY 219 (a) and for PRN 11 on DOY 300 (b) in 2011. In the bottom panels, the black curve is for S4, the red curve is for the conventional ROTI [10], the green curve is for the ROTI scaled using zonal drift velocity of irregularities derived from the VHF at Nairobi

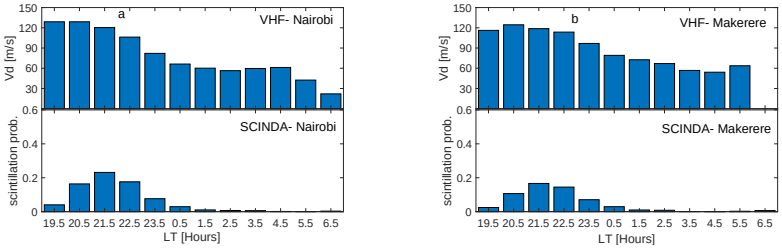

Fig. 3. Variation of hourly averaged zonal drift velocity of irregularities (top panels) and L-band scintillation (bottom panels) over Nairobi (a) in 2011 and Makerere (b) in 2012

The occurrence probabilities were determined by expressing the number of S4 values greater than 0.2 in an hour as a fraction of the total number of observations in a given time bin. The hourly averages presented in Fig. 3 are only for days where both L-band scintillation and zonal drift velocity data were available. Fig. 3 (a) shows that the maximum hourly averaged zonal drift velocity of irregularities over Nairobi is about 125 m/s between 19:00 LT and 21:00 LT in 2011. This velocity gradually decreased towards the local midnight. Similarly, Fig. 3 (b) shows that the peak zonal drift velocity of irregularities over Makerere was about 120 m/s and this was observed from 20:00 LT to 21:00 LT in 2012. The higher zonal irregularity drift velocity observed just after sunset is possibly a direct consequence of the post sunset enhancement in the thermospheric zonal neutral wind (U) due to pressure gradient at the terminator. In the case of the L-band scintillation observed from the nearest SCINDA receivers, Fig. 3 (a) shows that the highest likelihood of scintillation occurrence was between 21:00 LT and 22:00 LT, and the chances of occurrence of L-band scintillation significantly reduced almost to zero just after local midnight. A similar higher likelihood of L-band scintillation over Makerere was also observed to be between 21:00 LT and 22:00 LT. Similar to the case of Nairobi, the L-band scintillation ceased just after the local midnight. The enhanced post sunset thermospheric zonal neutral wind creates polarization electric fields through the $U \times B$ mechanism [26]. The polarization electric field has a prominent vertical component and a small zonal component [27]. The vertical component drives an eastward electric field. This electric field enhances the already eastward eveningtime electric field resulting in a rapid uplift of the F layer plasma by $E \times B$ mechanism. This creates necessary conditions for the growth of irregularities within the F layer. These irregularities are responsible for the observed scintillation. The decreased occurrence probabilities after local midnight is possibly due to the decreased electrodynamic processes in the ionosphere. In general, Fig. 3 shows that at the time of peak likelihood of occurrence of scintillation, the irregularities were observed to drift with a zonal velocity of about 120 m/s. This velocity was used as a typical zonal drift velocity of irregularities over the East African region to scale ROTI to obtain a proxy for S4. To validate the possibility of using a constant drift velocity to scale ROTI at both the crest and the trough of the equatorial ionization anomaly (EIA), we have shown in Fig. 4 a comparison between S4 and S4p derived using a drift velocity of 120 m/s.

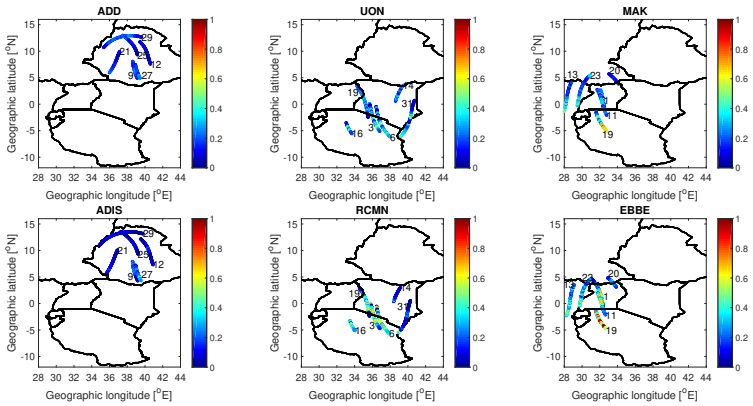

Fig. 4. Comparison between S4p with S4 over Addis Ababa, Nairobi and Makerere for DOY 157, 265 and 298 in 2011. The S4p was derived using a constant irregularities drift velocity of 120 m/s. The IPPs shown were observed between 19:00 LT and 06:00 LT at elevation angles greater than 30^o

From Fig. 4, mild scintillation events were observed at the SCINDA receiver ADD on PRNs 9, 27 and 29. The S4p from the nearby dual frequency GNSS receiver ADIS also showed values in the same range for all the visible satellites at elevation angles greater than 30^o. Particularly mild scintillation was observed on the same PRNs 9, 27 and 29 using the S4p index. At the SCINDA station UON which is near the crest region of the EIA, moderate scintillation was experienced by the signals on PRNs 3, 6, 14, 16,19 and 31. The S4p for the same PRNs from the nearby dual frequency GNSS receiver RCMN also revealed moderate scintillation, though S4p slightly over estimated S4 in some of the cases such as for PRNs 3, 6 and 19. Similarly for the case of the SCINDA receiver MAK, moderate scintillation was experienced by PRNs 1,11,13 and 23 and strong scintillation by PRN 19 on the evening of the DOY 298 in 2011. The S4p from the nearest dual frequency receiver EBBE also showed strong scintillation on PRN 19 and moderate scintillation on PRNs 1,11,13 and 23. In general, S4p is able to capture the spatial variation of scintillation over the East African region with stronger scintillation at the crest than at the trough of the EIA. The ability of S4p to capture the spatial scintillation characteristics over the region was investigated further by comparing the one minute S4p values with S4. The choice of one minute was to have the same sampling rate for S4p and S4. Fig. 5 shows the variation of the one minute averaged S4 and S4p for the different satellite geometries at elevation angles greater than 30^o over Addis Ababa, Makerere and Nairobi in 2011.

From Fig. 5, S4 values at ADD were smaller than those at MAK which in turn were less than what was observed at UON. Similarly, the S4p values were smallest at ADIS followed by EBBE and then RCMN. In all the cases, high values of S4 and S4p (S4, S4p $>$0.2) which signify scintillation activity were observed to peak between 20:00 LT and 23:00 LT. In some cases, S4p over estimated S4 especially near the crest of the EIA. Based on the the relatively good correlation between S4p and S4, and the good geographical coverage provided by the dual frequency GNSS receivers, we adopted S4p as an alternative for S4 to construct scintillation maps.

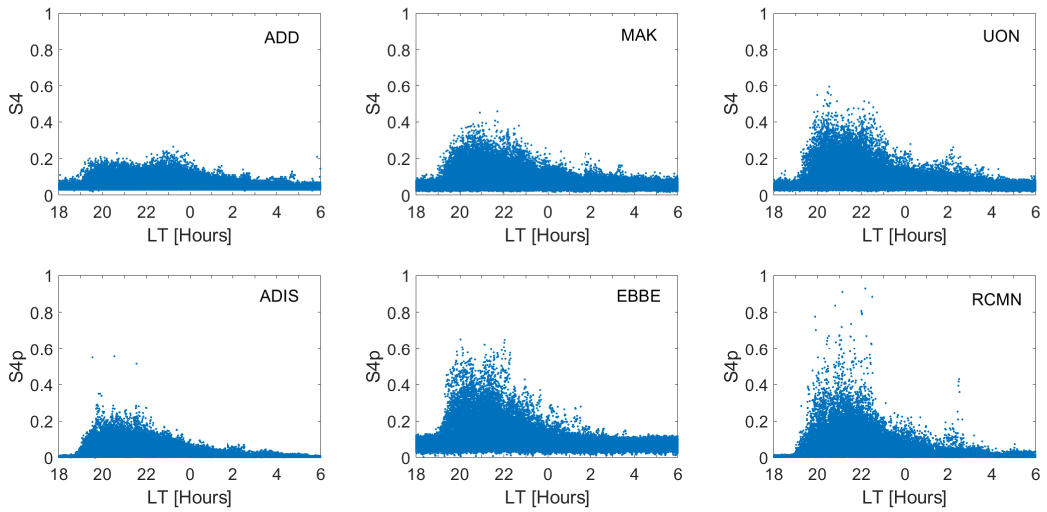

Fig. 5. Diurnal variation of S4 and S4p over Addis Ababa, Makerere and Nairobi in 2011

3.2 Scintillation Maps

3.2.1 Semivariogram

A semivariogram describes the relationship between the data points distributed in space. In Kriging, the semivariogram is important in selecting the appropriate sample weights. The starting point in semivariogram construction for Kriging is the empirical semivariogram to which an appropriate theoretical semivariogram is fitted. Before determining the experimental semivariogram, the S4p values within a latitude by longitude bin of $1^o \times 1^o$ were averaged. To determine the average, it was required that at least five values were present within the bin otherwise the bin was flagged to have no value. This averaging was necessary to minimize physically meaningless values of S4p. The average value of S4p in a given bin was then assigned to an IPP that was determined by inverse distance weighting of the different IPPs that fall within the bin. The bin averaged S4p values together with their corresponding IPP coordinates were then used to construct an empirical semivariogram. Fig. 6 shows a typical semivariogram for the DOY 300 in 2011 constructed using the S4p values between 16:30 UT and 21:00 UT generated for every thirty minutes.

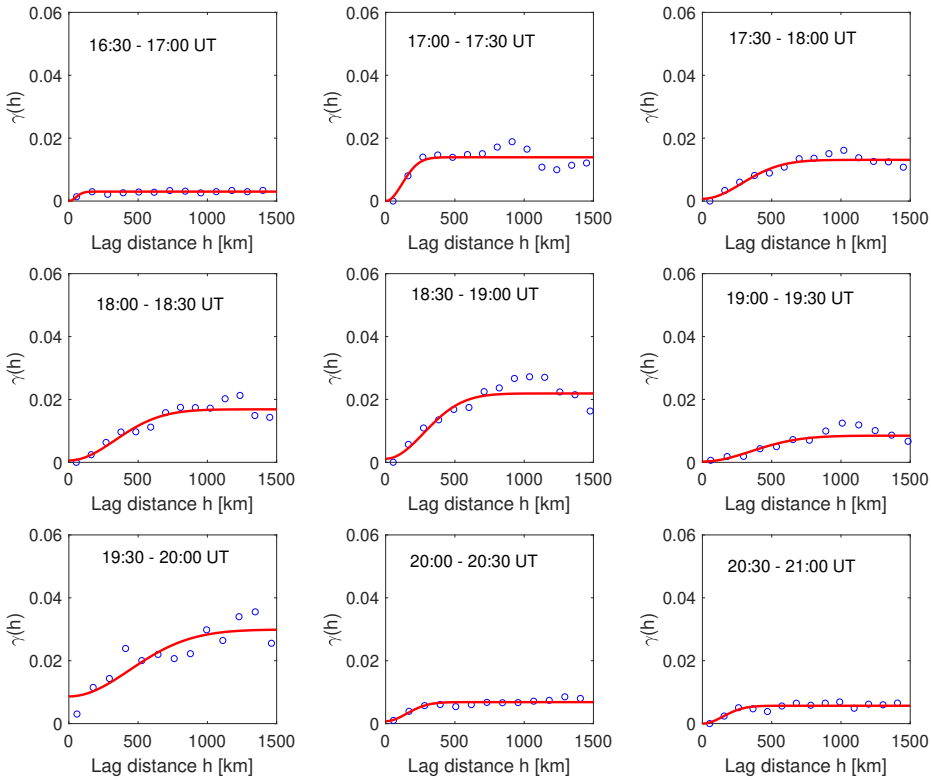

Fig. 6. Semivariogram for the ionospheric irregularities over the East African low latitude region observed from the S4p values on DOY 300 in 2011 between 16:30 UT and 21:00 UT. The blue dots are for the experimental semivariogram and the red curves are the fitted theoretical semivariogram.

The Kriging algorithm requires that the semivariogram function be positive definite and interpolatable. To meet these conditions, a theoretical semivariogram model is often used. The Kriging toolbox[1] used in this study offers a number of theoretical models such as linear, spherical, Gaussian and exponential that best describe a physical phenomena. The best theoretical semivariogram that matched the experimental semivariogram was determined by first calculating the root mean square error (RMSE) between the experimental and the theoretical semivariograms. The model with the least RMSE was then selected. In the study area, it was the Gaussian model given by

$$\gamma(h) = k_o + k\left(1 - e^{h^2/a^2}\right), \tag{11}$$

that produced the smallest error and therefore was chosen. The unknown parameters k_o, $k_o + k$ and a which represent the nugget, sill and range were determined from the S4p values for a given observation interval. The Gaussian semivariogram for each of the experimental semivariogram is shown with a solid line in Fig. 6. From Fig. 6, the nugget, sill and the range all show variation with time, particularly the sill value is high from 17:00 UT to 20:00 UT, the time when scintillation was observed over East Africa. Therefore all the parameters of the Gaussian semivariogram which we used to solve equation 9 for the Kriging weights λ_i were dynamical determined for each time interval. The Kriging weights were then applied in equation 6 to estimate the values of S4p at the un sampled points. The estimated values were then used to construct the scintillation maps over the region during quiet and disturbed conditions.

3.3 Example of a Scintillation Map on a Quiet Day

A typical quiet day of DOY 075 in 2011 when scintillation was observed over East Africa was chosen to demonstrate the ability of Kriging to generate S4p maps. Fig. 7 a (i) show that the minimum Disturbance storm time (Dst) index was just about -3 nT indicating that the day was quiet.

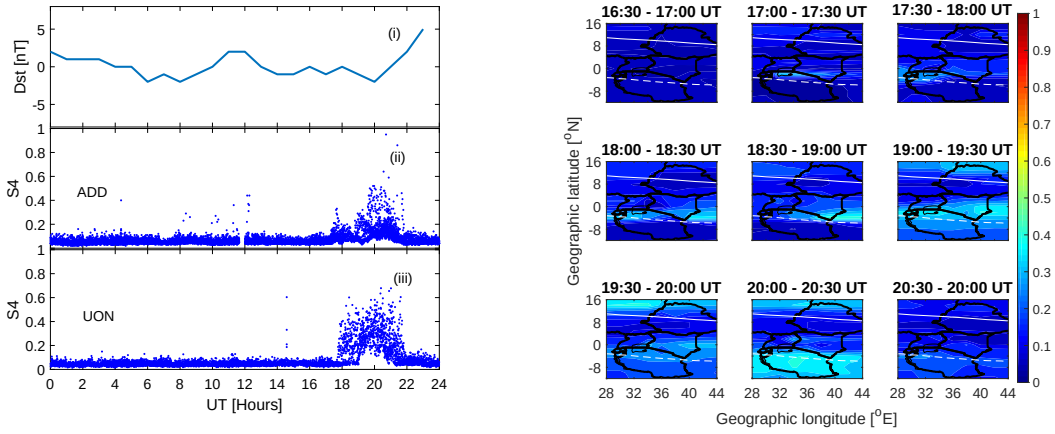

(a) **(b)**

Fig. 7. (a) Variation of Dst and S4 on DOY 075 in 2011. (b) Scintillation maps between 16:30 UT and 21:00 UT on DOY 075 in 2011

[1] https://sourceforge.net/projects/mgstat/files/mGstat/

The S4 from SCINDA receivers at Addis Ababa (ADD) and Nairobi (UON) show that there was scintillation over East Africa (see Fig. 7 a (ii) and (iii)). From Fig. 7 (a)(ii), scintillation over Addis Ababa started at about 19:00 UT and persisted up to about 21:00 UT with the peak occurrence at about 20:00 UT. Fig. 7 (a)(iii) shows that scintillation over Nairobi started earlier at about 18:00 UT with S4 reaching more than 0.4 between 18:00 UT and 21:00 UT. These observations suggest that scintillation at the crest region was stronger than that within the vicinity of the dip equator. The more pronounced scintillation near the crest of the ionization anomaly than around the dip equator could be due to the E$\times$B vertical drift of the ionospheric plasma at the dip equator which map the equatorial plasma together with the scintillation causing irregularities to the crest of the anomaly region. Fig. 7 (b) shows the scintillation maps over the East African region for the DOY 075 in 2011 generated from the S4p values by using the Gaussian semivariogram in the Kriging interpolation. The maps were generated in grid cells of $2^o \times 2^o$ in latitude by longitude. From the maps, scintillation at the crest of the EIA started at about 18:00 UT and ceased at about 20:30 UT. While at the trough, scintillation started between 19:00 and 19:30 UT and ceased between 20:00 and 20:30 UT. The time of maximum scintillation activity in the maps is consistent with the observation from the SCINDA receivers over the region showing that Kriging is a promising technique to generate scintillation maps over the region.

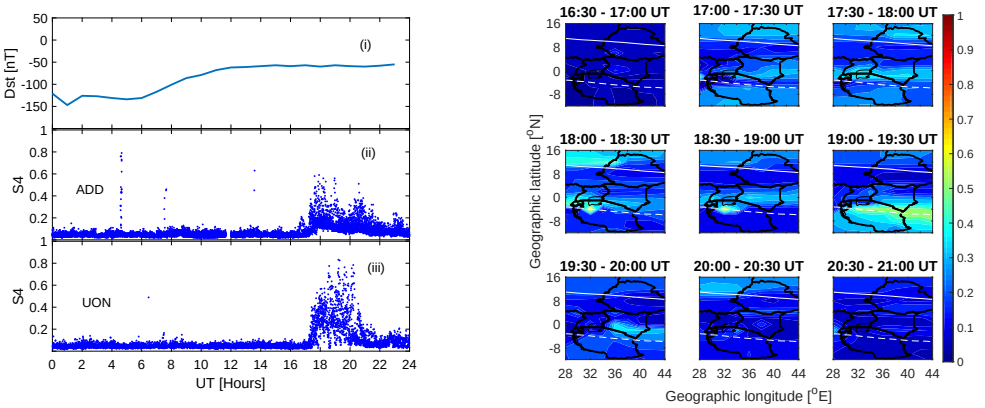

(a) **(b)**

Fig. 8. (a) Variation of Dst and S4 on DOY 298 in 2011. (b) Scintillation maps between 17:00 UT and 21:00 UT on DOY 298 in 2011

3.3.1 Example of a scintillation map on a disturbed day

A strong geomagnetic storm occurred between DOY 297 and DOY 299 with the main phase on DOY 298 in 2011. Fig. 8 (a) (i) shows that the Dst index reached a minimum value of -134 nT in the early hours of DOY 298 and the storm conditions (Dst $<$ -50 nT) persisted through out the day.

The variation of S4 index on the same day from the SCINDA receivers ADD and UON are shown in Fig. 8 (a) (ii) and (iii) respectively. The S4 values show that post sunset scintillation were observed both at the trough (ADD) and the crest (UON) on the storm day. The scintillation activity at the crest was stronger than that at the trough. Fig. 8 (b) shows examples of scintillation maps for the DOY 298 in 2011 constructed using S4p from 14 GNSS receivers since MBAR and BDAR had no data on the same day. The maps

show that scintillation started from about 17:30 to 18:00 UT and lasted for about one hour and significantly reduced between 18:30 and 19:00 UT. From about 19:00 to 19:30 UT, scintillation peaked and ceased between 19:30 and 20:00 UT. During the time of the peak scintillation activity, S4p reached a value of more than 0.5. This again is in agreement with the observations from the SCINDA receivers. This further affirms that S4p may be used to map scintillation over East Africa during storm conditions when an appropriate interpolation technique such as Kriging is used.

3.3.2 Validation of the scintillation maps

To validate the scintillation maps, we compared the S4 values for some selected PRNs that were visible at elevation angles greater than 30^o on the DOY 263 from the SCINDA receivers at Addis Ababa, Makerere and Nairobi with the S4p values generated by Kriging interpolation. The values simulated from the Kriging interpolation were at the location of the IPP coordinates of the PRNs observed at the SCINDA receiver sites. Fig. 9 shows the results for PRN 11 observed at Addis Ababa and Nairobi, and PRN 19 observed at Makerere.

The simulated values show a good correlation with the S4 observed from the SCINDA receivers. However, the inherent assumption of stationarity of the mean applied in the Kriging algorithm tends to smooth out some of the extreme values of S4p. This shortfall can be traded off with the advantage offered by the scintillation maps in space weather monitoring. We further simulated the S4p values for all the PRNs that were visible in the evening of DOY 075 and DOY 298 at elevation angles greater than 30^o and then determined the Pearson correlation coefficients between these values with the S4 values from the SCINDA receivers. Fig. 10 shows the results for the correlation analysis at Addis Ababa, Makerere and Nairobi.

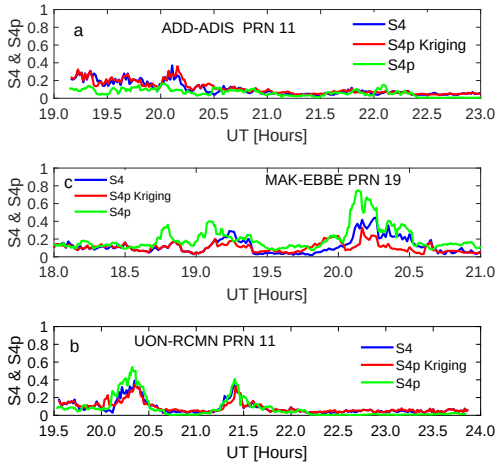

Fig. 9. Comparison between S4, S4p and simulated S4p on the evening of DOY 263 in 2011 over Addis Ababa, Makerere and Nairobi.

From Fig. 10, the simulated S4p by Kriging show a good positive correlation with correlation coefficients between $\sim$0.9055 and $\sim$0.9689 with the S4. Therefore the maps will provide a good estimate for S4 at the un sampled positions and may be useful in understanding spatio-temporal evolution of scintillation patterns.

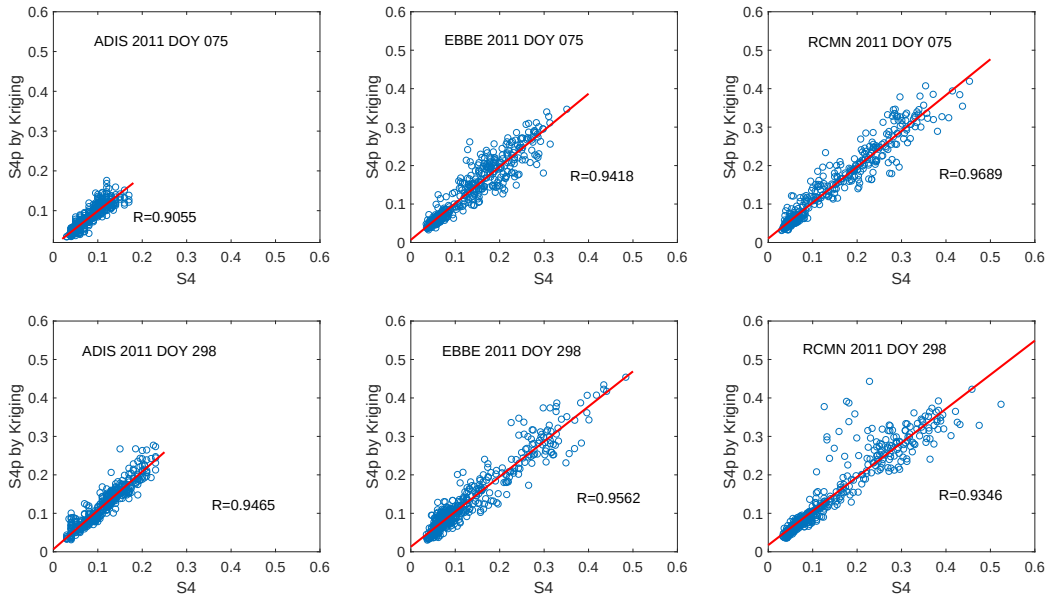

Fig. 10. Correlation analysis between S4 and the interpolated S4p over Addis Ababa, Makerere and Nairobi on the evening of DOY 075 and DOY 298 in 2011

4 CONCLUSION

Ordinary Kriging algorithm is used to generate amplitude scintillation maps over the East African region using a scintillation proxy data from 16 dual frequency GNSS receivers over the region. The data from the GNSS receivers was used to derive ROTI which is then scaled to obtain a more numerically accurate proxy for amplitude scintillation referred to here as S4p. The proxy is validated against S4 derived from nearly collocated SCINDA receivers over the region. The S4p is then used to generate amplitude scintillation maps by using the Kriging interpolation technique. The features observed in these maps were consisted with what is observed from the SCINDA receivers. These observations show that the Kriging algorithm is a promising method to produce scintillation maps over East Africa. The maps generated from the scintillation proxy can be used to study the spatio-temporal evolution of scintillation and hence scintillation causing irregularities.

ACKNOWLEDGEMENT

The SCINDA receivers from which the scintillation data used in this study were obtained, were supplied by the Air Force Research Laboratory in coordination with Boston College, USA. The GNSS data used in this study was obtained from ftp://cddis.gsfc.nasa.gov/ and ftp://data-out.unavco.org/pub/-rinex/. The precise orbit files which we used to calculate the ray path velocities were obtained from ftp://ftp.nga.mil/pub2/gps/apcpe/.

COMPETING INTERESTS

Authors have declared that no competing interests exist.

REFERENCES

[1] Klobuchar A. Ionospheric time-delay algorithm for single-frequency gps users. IEEE Trans. 1983;23:325–331.

[2] Mengyang Z, Baowei L, Wenmiao S. A method for dual frequency ionospheric time delay correcting using a C/A code GPS receiver. Journal of electronics. 1999;16:66–72.

[3] Hofmann-Wellenhof B, Lichtenegge H, Wasle E. Global Navigation Satellite Systems, GPS, GLONASS, Galileo and More. Springer Wien New York; 2008.

[4] Kintner P, Ledvina B M, de Paula ER. GPS and ionospheric scintillation. Space Weather. 2007;5:S09003.

[5] Iyer KN, Souza JR, Pathan BM, Abdu MA, Jivani MN, Joshi HP. A model of equatorial and low latitude VHF scintillation in India. Ind. J. Radio and Space Phys. 2006;35:98-104.

[6] Frernouw EJ, Secan JA. Modeling and scientific application of scintillation result. Radio Sci. 1984;19:687-694.

[7] Rino CL. A power law phase screen model for ionospheric scintillation: 1. weak scatter. Radio Sci. 1979;14:1135-1145.

[8] Priyadarshi S. A review of ionospheric scintillation models. Surv. Geophys. 2015;36:295–324.

[9] Caton RG, McNeil WJ. GPS proxy model for real-time UHF satellite communications scintillation maps from the Scintillation Network Decision Aid (SCINDA). Radio Sci. 2004;39:RS1S22.

[10] Pi X, Mannucci AJ, Lindqwister UJ, Ho CM. Monitoring of global ionospheric irregularities using the worldwide GPS network. Geophys. Res. Lett. 1997;24:2283-2286.

[11] Basu S, Groves KM, Quinn JM, Doherty P. A comparison of TEC fluctuations and scintillations at Ascension Island. J. Atmos. Sol.-Terr. Phys. 1999;61:1219-1226.

[12] Du J, Wilkinson P, Thomas R, Cerver M. Determination of equatorial ionospheric scintillation S4 dual frequency GPS. URSI Commission G, Workshop, La Trobe University, Australia; 2000.

[13] Prikryl P, Ghoddousi-Fard R, Kunduri BSR, Thomas EG, Coster AJ, Jayachandran PT, Spanswick E, Danskin DW. GPS phase scintillation and proxy index at high latitudes during a moderate geomagnetic storm. Ann. Geophys. 2013;31:805–816.

[14] Amabayo EB, Jurua E, Cilliers PJ. Validating the use of scintillation proxies to study ionospheric scintillation over the Ugandan region. J. Atmos. Sol.-Terr. Phys. 2015;128: 84-91.

[15] Andima G, Amabayo EB, Jurua E, Cilliers PJ. GPS derived amplitude scintillation proxy model: A case over a low latitude station in east africa. J. Atmos. Sol.-Terr. Phys. 2020;211. Available:https://doi.org/10.1016/j.jastp.2020.105461

[16] Seemala GK, Valladares C. Statistics of total electron content depletions observed over the south american continent for the year 2008. Radio Sci. 2011;46:RS5019.

[17] Carrano CS, Groves KM, Rino CL. On the relationship between the rate of change of total electron content index (ROTI), irregularity strength (C_kL), and the scintillation index (S_4). J. Geophys. Res.: Space Phys. 2019;124:2099-2112.

[18] Krige D G. A statistical approach to some basic mine valuation problems on the witwatersrand. Journal of the Chemical and Metallurgical Society of South Africa. 1951;52:119-139.

[19] Oliver MA, Webster R. Basic Steps in Geostatistics: The Variogram and Kriging. Springer Science and Business Media; 2015.

[20] Huang L, Zhang H, Xu P, Geng J, Wang C, Liu J. Kriging with unknown variance components for regional ionospheric reconstruction. Sensors. 2017;17(3):468.

[21] Abe O, Rabiu A, Bolaji O, Oyeyemi E. Modeling African equatorial ionosphere using ordinary kriging interpolation technique for gnss applications. Astrophys Space Sci. 2018;363(168). Available:https://doi.org/10.1007/s10509-018-3387-x

[22] Hamel P, Sambou DC, Darces M, Beniguel Y, Helier M. Kriging method to perform scintillation maps based on measurement and gism model. Radio Sci. 2014;49:746-752.

[23] Harsha PBS, Ratnam DV, Nagasri ML, Sridhar M, Raju KP. Kriging-based ionospheric tec, roti and amplitude scintillation index (s4) maps for india. IET Radar Sonar Navig. 2020;14:1827-1836.

[24] Geng W. Huang W, Liu G, Aa E, Liu S, Chen Y, Luo B. Generation of ionospheric scintillation maps over southern china based on kriging method. Adv. Space Res. 2020;65:2808-2820.

[25] Kintner PM, Ledvina BM, de Paula ER, Kantor IJ. Size, shape, orientation, speed, and duration of gps equatorial anomaly scintillations. Radio Sci. 2004;39:RS2012.

[26] Rishbeth H. Thermospheric winds and the f-region: A review. J. Atmos. Terr. Phys. 1972;34:1-47.

[27] Heelis R. Electrodynamics in the low and middle latitude ionosphere:a tutorial: J. Atmos. Sol.-Terr. Phys. 2004;66:825-838.

Peer-review history:
The peer review history for this paper can be accessed here:
http://www.sdiarticle4.com/review-history/66815